 LBL-27012

Lawrence Berkeley Laboratory
UNIVERSITY OF CALIFORNIA

Presented at the International Conference
"Fifty Years of Research in Nuclear Fission,"
Berlin, Germany, April 3–7, 1989, and
to be published in Nuclear Physics A

Angular-Momentum-Bearing Modes in Fission

L.G. Moretto, G.F. Peaslee, and G.J. Wozniak

March 1989

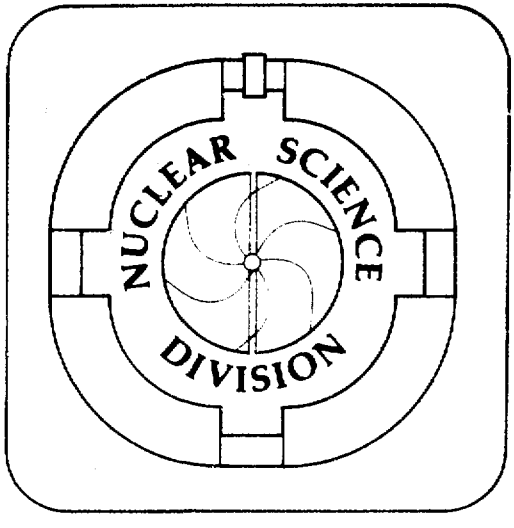

Prepared for the U.S. Department of Energy under Contract Number DE-AC03-76SF00098.

LBL--27012

DE89 011779

ANGULAR - MOMENTUM - BEARING MODES IN FISSION

Luciano G. Moretto, Graham F. Peaslee, and Gordon J. Wozniak

Nuclear Science Division, Lawrence Berkeley Laboratory, 1 Cyclotron Rd., Berkeley, CA 94720

The angular-momentum-bearing degrees of freedom involved in the fission process are identified and their influence on experimental observables is discussed. The excitation of these modes is treated in the "thermal" limit and the resulting distributions of observables are calculated. Experiments demonstrating the role of these modes are presented and discussed.

1. INTRODUCTION

The appreciation of the role of angular momentum in fission can be described as a punctuated evolution of ideas, some indigenous to the field itself, some borrowed from allied disciplines. The discovery of a critical stage in fission, involving the passage of the system through a deformed configuration (saddle point) by the negotiation of a barrier, brought to light the associated "rigid" rotational modes. The application of angular momentum to one such mode, through rotation about an axis perpendicular to the elongation axis, led to the conclusion that fission barriers would decrease and eventually vanish with increasing angular momentum. Quantitative predictions of such a dependence were obtained within the framework of the liquid drop model[1].

The analogy of the axially symmetric nucleus at the saddle point with deformed ground state nuclei suggested a "rotational" spectroscopy in the saddle-point transition state. The assumption of conservation of the K quantum number from saddle to scission prompted attempts to study this spectroscopy by means of fission-fragment angular distributions[2]. Evidence for discrete rotational bands in the transition state of nuclei in the U - Th region was reported in low-energy fission induced by neutrons[3], gammas[4], etc. At higher excitation energies, the introduction of the statistical distribution in K quantum numbers and the connection of its variance (K_0^2) to the nuclear temperature and to the principal moments of inertia at the saddle point, led to the classical theory of fission-fragment angular distributions as developed by Halpern and Strutinski[5].

So much about the "rigid" rotor degrees of freedom. The possibility that other intrinsic angular-momentum-bearing modes could be active in the fission process surfaced with the early observation of a sizeable amount of angular momentum (and aligned, at that!) in fission fragments from the spontaneous fission of ^{252}Cf[6]. The magnitude of the fragment angular momentum (~7$\hbar$ / fragment) despite the 0^+ ground state of the parent suggested a prescission origin and thus the involvement of non-rigid modes. A listing of such modes at the saddle point can be found in the thesis work of Nix[7], but their major involvement with the fragment angular momentum had to wait for the advent of heavy ion reactions.

The lesson of heavy ion reactions was both extensive and incisive. Deeply inelastic reactions showed that the entrance-channel orbital angular momentum could be dissipated in a continuous fashion all the way down to the rigid rotation limit[8,9]. This implied the existence of an intrinsic mode coupling the orbital angular momentum to the spins of both fragments. The "wriggling" mode, described below, satisfies this requirement. Further studies of the magnitude of the fragment spins by means of γ-ray multiplicity measurements suggested that the fragments had angular momenta in excess of what was expected from rigid rotation[10]. The explanation was found in the (diffusive or thermal) excitation of additional intrinsic angular-momentum-bearing modes.

A beautiful confirmation of the excitation of these modes came from the misalignment of the fragment spins. The key experiments were the measurements of fragment γ-ray angular distributions[11-20], sequential particle evaporation[21-24], and sequential-fission-fragment angular distributions[25-30]. Such a misalignment was shown to arise from the coupling of the aligned angular momentum component associated with rigid rotation to that associated with the random fluctuations of those intrinsic modes, whose angular momentum is perpendicular to the rigid rotation component[31].

A framework for a global interpretation of these phenomena was offered in the work of Moretto and Schmitt[31,32], where the angular-momentum-bearing modes in a symmetric dinuclear system were illustrated, and their statistical mechanics worked out. There are five intrinsic modes: two wriggling modes, two bending modes, and one twisting mode, plus the tilting mode arising from the angle between the total angular momentum and the symmetry axis. On this basis, a large amount of data from heavy ion reactions found a rational and systematic explanation.

Another degree of freedom that, while unable to carry angular momentum, is deeply affected by it, and requires some attention, is the mass-asymmetry degree of freedom. Recently this degree of freedom has come into the limelight because of its dominant role in the compound nucleus emission of complex fragments[33,34]. This process has been described as an asymmetric mode of decay controlled by an associated conditional barrier[33]. The saddle point in this description is a conditional saddle, because the mass asymmetry is assumed to be frozen. The locus of these conditional barriers along the mass asymmetry mode coordinate is called the ridge line. Since the seminal work of Businaro and Gallone[35], it was appreciated that the topology of the ridge line changes from low x values to large x values, the mass asymmetry mode evolving from stability to instability as the fissility parameter x is decreased across the "Businaro-Gallone" point (x_{BG}=0.396). The Businaro-Gallone point was also found to decrease with increasing angular momentum[1]. As a consequence, drastic changes are produced in the fragment mass distributions as the angular momentum is increased. Furthermore, the mass asymmetry parameter strongly affects the nature and importance of the intrinsic angular-momentum-bearing modes. In particular, the tilting mode becomes very soft with increasing mass asymmetry. A thorough study of the mass asymmetry dependence of these modes has been carried out by Schmitt and Pacheco[36], as a generalization of the theory presented by Moretto and Schmitt[31] for symmetric dinuclear systems.

Finally, in recent times there has been a revisitation of the rigid rotation modes in the study of

fission-fragment angular distributions associated with heavy-ion-induced fission[37-46]. These studies have demonstrated that the K quantum number may not be frozen at the saddle point after all, but may be determined at scission, or somewhere in between. This opens up a problem that has never been truly solved, namely whether this and the other angular-momentum-bearing modes are thermally or dynamically excited, and, if they are thermally excited, whether the statistical equilibrium relevant for the description of the various observables is at the saddle or at the scission point. A great deal of information bearing on this problem is about to be released from the study of the fission fragment spins obtained by means of the latest, most powerful techniques made available by high spin spectroscopy[47]. So, despite the large amount of work performed in the first half century of fission, there seems to be enough work left for a second half century.

2. THE DINUCLEAR SYSTEM: ITS DEGREES OF FREEDOM AND STATISTICAL MECHANICS

If the nucleus at the saddle point (or for that matter, at the scission point) is considered as a single rigid body, it can be characterized by a total of six degrees of freedom: three translational modes associated with the motion of the center of mass, and three rotational modes. Furthermore, if the nucleus is axially symmetric, as it is commonly assumed, the three rotational degrees of freedom can be reduced to a rotation about the symmetry axis, plus a (doubly degenerate) rotation about an axis perpendicular to the symmetry axis. This requires that the component K of the angular momentum along the symmetry axis be a constant of motion. Thus, the angle between the angular momentum and the symmetry axis is conserved; because of its relevance, such an angle is called the "tilting" angle.

The experimental measurements of fragment angular momentum[11-30], and its alignment, indicate the relaxation of the rigid body condition, and require the introduction of intrinsic angular-momentum-bearing modes characteristic of a dinuclear system. These modes are easily visualized for a symmetric dinuclear system constituted by two equal spheres in contact[31], although the generalization to an asymmetric system of two touching, unequal spheroids is rather straightforward.

The enumeration of the degrees of freedom of a dinuclear system is immediate: two rigid bodies require 6+6=12 degrees of freedom. The condition of contact removes one, which leaves eleven. Of these, three are translational degrees of freedom, so there are eight angular-momentum-bearing modes left. Of these, three are associated with the "rigid" rotation of the dinuclear system. The remaining five degrees of freedom are "intrinsic" angular-momentum-bearing modes. These modes are associated with rotations of one nucleus with respect to the other in such a way that the whole system need not carry a net amount of angular momentum. The five normal modes (plus the tilting mode) are illustrated in figure 1. They are: two degenerate "bending" modes, two degenerate "wriggling" modes and one "twisting" mode. These names have been chosen to correspond with the normal modes at the saddle point as described by Nix[7], although the correspondence is not completely obvious.

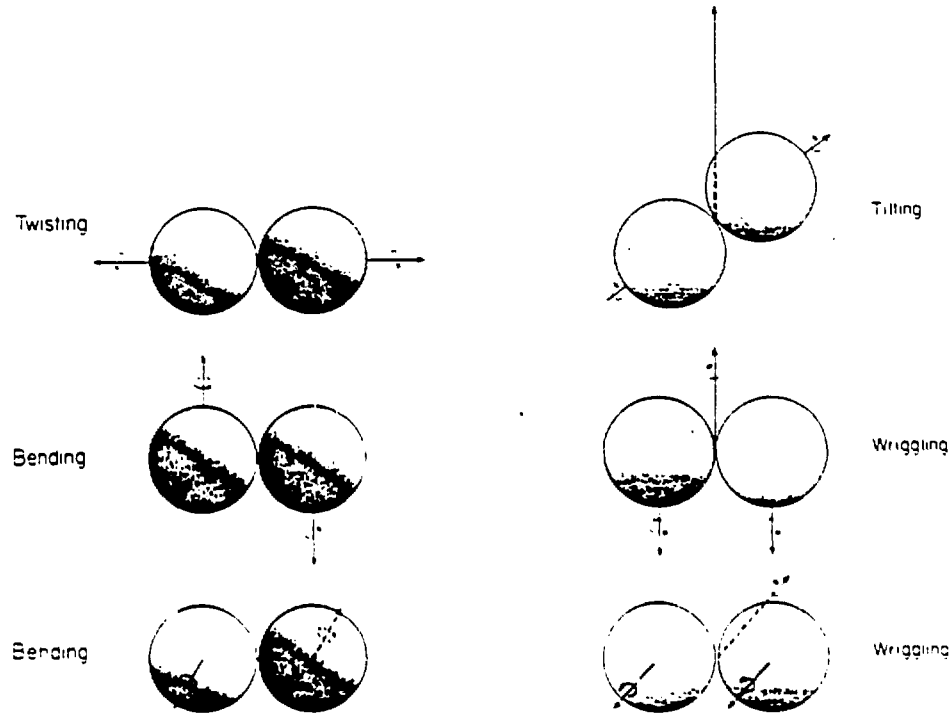

Figure 1. *(Left)* Schematic illustrating the twisting and the doubly degenerate bending modes for a two-equal-spheres model. In each case the spin vectors of the fragments (symbolized by the shorter arrows) are of equal length but point in opposite directions. *(Right)* Schematic illustrating the tilting mode and the doubly degenerate wriggling modes for a two-equal-spheres model. The long arrows originating at the point of tangency of the two spheres represents the orbital angular momentum vectors[31].

The bending mode consists in the rotation of one sphere about an axis perpendicular to the symmetry axis, and in the corresponding *counterrotation* of the other sphere. This mode is doubly degenerate.

The twisting mode consists in the rotation of one sphere about the symmetry axis, and in the corresponding *counterrotation* of the other sphere. This mode is not degenerate.

The wriggling mode is somewhat more complicated. Both spheres *corotate* about parallel axes perpendicular to the symmetry axis, and simultaneously *counterrevolve* about each other about an axis parallel to the rotation axes. This mode is doubly degenerate.

In the bending and twisting modes, the spin of one sphere is compensated by that of the other, so that the net angular momentum is always zero. In the wriggling modes, the spins of the two spheres are equal and parallel, and they are exactly compensated by the orbital angular momentum associated with the revolution which is antiparallel to the fragment spins. Therefore, the excitation of the bending and twisting modes produces fragment spins which are antiparallel, while the excitation of the wriggling (and tilting) modes produces fragment spins that are parallel.

2.1. Statistical Coupling Between Orbital and Intrinsic Angular Momenta: The Wriggling Modes

As we have mentioned above, the coupling between orbital and intrinsic angular momentum is mediated by one wriggling mode. This is illustrated in figure 2, where it is shown that the addition of orbital motion to an excited wriggling mode leads to a decrease of the orbital and to an increase of the intrinsic angular momentum.

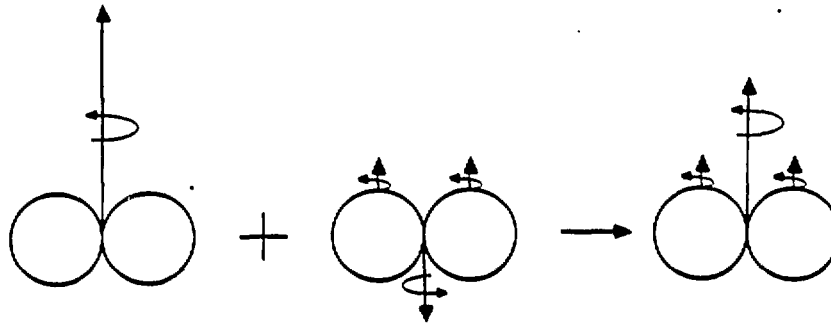

Figure 2. Schematic showing how the addition of orbital angular momentum (symbolized by the long arrow) to an excited wriggling mode leads to a decrease of the orbital angular momentum and an increase of the intrinsic angular momentum.

If the total angular momentum is I and the fragment spin is s, the energy for an arbitrary partition between orbital and intrinsic angular momentum is:

$$E(s) = \frac{(I-2s)^2}{2\mu r^2} + \frac{2s^2}{2\Im} = \left[\frac{2}{\mu r^2} + \frac{1}{\Im}\right] s^2 - \frac{2I}{\mu r^2} s + \frac{I^2}{2\mu r^2} . \qquad (1)$$

The first term is the orbital and the second is the intrinsic rotational energy, $\Im$ being the moment of inertia of one of the two equal spheres. The partition function is:

$$Z \propto \int e^{-E(s)/T} \, ds = \sqrt{\frac{\pi \mu r^2 \Im T}{2\Im + \mu r^2}} \exp\left[-\frac{I^2}{2T(2\Im + \mu r^2)}\right] . \qquad (2)$$

The average spin for both fragments is given by:

$$2\bar{s} = \frac{2\int s\, e^{-E(s)/T} ds}{Z} = \frac{2\Im}{\mu r^2 + 2\Im} I = \frac{2}{7} I = 2 I_R . \qquad (3)$$

This is, of course, the rigid rotation limit. The second moment $\overline{s^2}$ is given by:

$$4\overline{s^2} = \frac{2\mu r^2 \Im T}{\mu r^2 + 2\Im} + \frac{4 I^2 \Im^2}{(\mu r^2 + 2\Im)^2} . \qquad (4)$$

From this we obtain the standard deviation:

$$4\,\sigma_s^2 = \frac{2\Im \mu r^2 T}{\mu r^2 + 2\Im} = \frac{10}{7} \Im T . \qquad (5)$$

The result in (3) is temperature independent, as one should expect from the fact that (1) is quadratic in s. This result could be obtained by solving the equation:

$$\frac{dE}{ds} = 0 . \tag{6}$$

This result corresponds to the mechanical limit of *rigid rotation* when the orbital and the intrinsic angular velocities are matched.

The result in (5) could have been obtained also by appreciating that the thermal fluctuations about the average in (3) are controlled by the second derivative of (1) at the minimum, or:

$$4\,\sigma_s^2 = 4\,T/b \tag{7}$$

where:

$$b = \left[\frac{\partial^2 E}{\partial s^2}\right]_{\bar{s}} . \tag{8}$$

In the case of $I = 0$, the fragments are still going to acquire angular momentum as shown by (4):

$$\overline{s^2} = \frac{1}{2}\,\frac{\mu r^2\,\Im\,T}{\mu r^2 + 2\Im} = \frac{5}{14}\,\Im\,T . \tag{9}$$

Since there are *two* wriggling modes, the mean square angular momentum of each fragment is:

$$\overline{S^2} = 2\,\overline{s^2} = \frac{\mu r^2\,\Im\,T}{\mu r^2 + 2\Im} = \frac{5}{7}\,\Im\,T . \tag{10}$$

2.2. The Bending and Twisting Modes

These three degrees of freedom are illustrated in figure 1. They are degenerate in our two-equal-sphere model. A splitting of the degeneracy could easily occur in the case of fragment deformation. We shall not consider this important possibility at the moment, although it is completely trivial, because of the arbitrariness in the choice of deformation.

The partition function for these three degenerate modes can be written as:

$$Z \propto \int R^2\, e^{-\frac{R^2}{\Im T}}\, dR , \qquad \ln Z = A - \frac{3}{2}\ln\frac{1}{\Im T} \tag{11}$$

from which :

$$\overline{R} = 2\sqrt{\frac{\Im\,T}{\pi}} , \qquad \overline{R^2} = -\frac{\partial \ln Z}{\partial\left[\frac{1}{\Im T}\right]} = \frac{3}{2}\,\Im T \tag{12}$$

or 1/2 $\Im T$ per degree of freedom.

Notice that R is the angular momentum of *each* fragment and that, for each mode, the angular momenta of the two fragments cancel out pairwise. Furthermore, for each fragment the resulting

angular momentum is randomly oriented. It is worth stressing again that, as for the wriggling modes, this angular momentum can exist even when the total angular momentum is zero because of the pairwise cancellation mentioned above.

At this point the (frequently asked) question may arise: "The bending and twisting modes in the two sphere model have no restoring force. Wouldn't the results be different if we were to introduce them?" The answer is no. Neglecting the degeneracy for the moment, the Hamiltonian would look like:

$$H = \frac{R^2}{\Im} + \frac{1}{2} k \omega^2 \tag{13}$$

where ω is the conjugate angle and k is the stiffness. The partition function thus factors the kinetic and potential energy components:

$$Z = \int e^{-\frac{R^2}{\Im T}} dR \int e^{-\frac{k\omega^2}{2T}} d\omega \quad . \tag{14}$$

As a consequence, any moment of R is strictly independent of the value of the stiffness k.

2.3. The Tilting Mode

This mode is unlike the other five "intrinsic" modes in the sense that it cannot confer angular momentum to the fragments, while keeping the total angular momentum equal to zero. However, we treat its statistical mechanics here because of its importance.

In their most stable configuration, the two touching fragments are aligned with their common axis perpendicular to the total angular momentum. Because of thermal fluctuations, this condition can be relaxed. If we now assume that the two fragments are rigidly attached one to the other, the energy is given by:

$$E = \frac{I^2 - K^2}{2\Im_\perp} + \frac{K^2}{2\Im_{||}} = \frac{I^2}{2\Im_\perp} + \frac{K^2}{2\Im_{eff}} \tag{15}$$

where $\Im_\perp = 2\Im + \mu r^2$, $\Im_{||} = 2\Im$ and $\Im_{eff}^{-1} = \Im_{||}^{-1} - \Im_\perp^{-1}$; K is the projection of the angular momentum I along the line of centers. The partition function is:

$$Z = \sqrt{\pi} \exp\left[-\frac{I^2}{2\Im_\perp T}\right] \sqrt{2\Im_{eff} T} \; \mathrm{erf}\left[\frac{I}{\sqrt{2\Im_{eff} T}}\right] , \tag{16}$$

from which:

$$\overline{K^2} = \Im_{eff} T - \frac{I\sqrt{2\Im_{eff} T}}{\sqrt{\pi}} \frac{\exp\left[-\frac{I^2}{2\Im_{eff} T}\right]}{\mathrm{erf}\left[\frac{I}{\sqrt{2\Im_{eff} T}}\right]} . \tag{17}$$

For small I we have:

$$\overline{K^2} = \frac{1}{3} I^2 , \tag{18}$$

while for large I we have:

$$\overline{K^2} = \Im_{eff} T = \frac{14}{5} \Im T . \tag{19}$$

The total fragment spin is given by:

$$2s = \sqrt{K^2 + \frac{4}{49}\left[I^2 - K^2 \right]} \tag{20}$$

and the averaged square quantity is:

$$4\overline{s^2} = \overline{K^2} + \frac{4}{49} I^2 - \frac{4}{49}\overline{K^2} = \frac{45}{49}\overline{K^2} + \frac{4}{49} I^2 \tag{21}$$

and for large I:

$$4\overline{s^2} = \frac{18}{7} \Im T + \frac{4}{49} I^2 . \tag{22}$$

2.4. Summary and Generalization to Asymmetric Dinuclear Systems

The overall statistical treatment of the angular-momentum-bearing modes allows us to describe the angular momentum distribution of one of the two fragments as a tridimensional Gaussian distribution in the angular momentum components I_x, I_y, I_z:

$$P(I) \propto \exp - \left[\frac{I_x^2}{2\sigma_x^2} + \frac{I_y^2}{2\sigma_y^2} + \frac{(I_z - \overline{I}_z)^2}{2\sigma_z^2} \right] , \tag{23}$$

where I_z is the rigid rotation component:

$$\overline{I}_z = \frac{\Im_i}{\mu r^2 + 2\Im_i} I = \frac{1}{7} I \tag{24}$$

for equal touching spheres, and:

$$\sigma_x^2 = \sigma_{twist}^2 + \sigma_{tilt}^2 = \frac{1}{2} \Im T + \frac{7}{10} \Im T = \frac{6}{5} \Im T \tag{25}$$

$$\sigma_y^2 = \sigma_{bend}^2 + \sigma_{wrig}^2 = \frac{1}{2} \Im T + \frac{5}{14} \Im T = \frac{6}{7} \Im T \tag{26}$$

$$\sigma_z^2 = \sigma_{bend}^2 + \sigma_{wrig}^2 = \frac{1}{2} \Im T + \frac{5}{14} \Im T = \frac{6}{7} \Im T . \tag{27}$$

In the case of an asymmetric system, the results are qualitatively similar[36]. The three variances in dimensionless units are shown in figure 3 as a function of mass asymmetry for two touching spheres. The most remarkable feature of this figure is the rapid increase of the variance σ_x^2 with increasing asymmetry. This effect is almost exclusively due to the softening of the tilting mode.

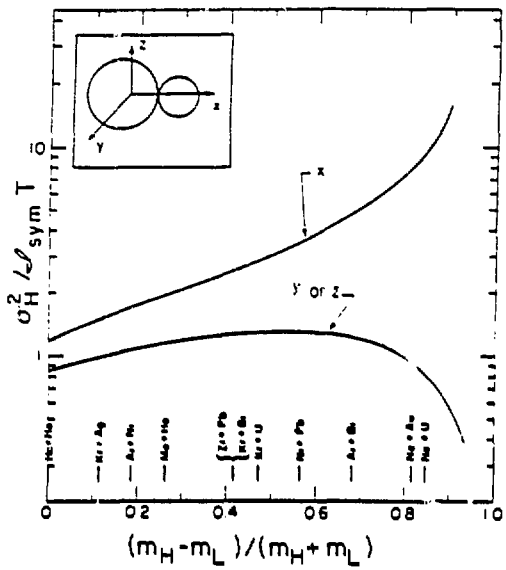

Figure 3. The heavy fragment spin variances for a dinuclear complex are shown as a function of mass asymmetry. The variances are shown in dimensionless units after division by $\mathcal{I}_{sym}T$, the moment of inertia of a mass symmetric spherical fragment times the temperature[60].

As one of the two spheres becomes smaller, the rotational energy increase associated with an increasing projection K becomes smaller. The corresponding K_0^2 increase for the very asymmetric configurations associated with the emission of an alpha particle, a proton, or a neutron is responsible for the small anisotropy in the angular distributions of these particles in comparison with those for symmetric fission.

3. ANGULAR MOMENTUM DEPENDENCE OF THE FISSION BARRIERS AND THE MASS ASYMMETRY COORDINATE

The decrease of the fission barrier height with increasing angular momentum, and its eventual disappearance, was appreciated by the earliest studies based upon the liquid drop model. The classical work by Cohen, Plasil and Swiatecki[1] describes all the stationary points of a rotating liquid drop potential-energy surface in terms of two dimensionless parameters:

$x = (E_{coulomb}/2E_{surface})$; $y = (E_{rot}/E_{surface})$

where the various energies, $E_{coulomb}$, E_{rot}, and $E_{surface}$ are calculated for the equivalent spherical configuration. However, the topology of the potential energy surface with explicit incorporation of mass asymmetry was already understood in the pioneering work of Businaro and Gallone[35]. Within the two sphere model, the symmetric saddle point is unstable (degree of instability 2) below the value $x = x_{BG}$ ($x_{BG} = 0.396$ in the liquid drop model and $x_{BG} = 0.6$ for two touching spheres at $y = 0$). For $x > x_{BG}$ the saddle point branches out into three new saddles: one, at symmetry, is stable with respect to the mass-asymmetry mode (degree of instability 1), and the other two move out at mirror asymmetry and have degree of instability 2. They are sometimes vividly called Businaro-Gallone mountains. This topology is retained at higher angular momentum, with the Businaro-Gallone point decreasing with increasing angular momentum. More recently, the association of the ridge line (locus of conditional saddle points at fixed mass asymmetry) with complex fragment emission[33-34] has prompted the calculation of the potential energy surface as a function of mass asymmetry, using both the liquid drop model and the finite range model[48]. The latter model, an improvement upon the liquid drop model, explicitly treats the surface-surface interaction that is so important for highly necked-in configurations.

An example of the overall dependence of the fission barrier upon angular momentum and mass asymmetry is shown in figure 4. The calculation has been performed for the nucleus ^{110}Sn with

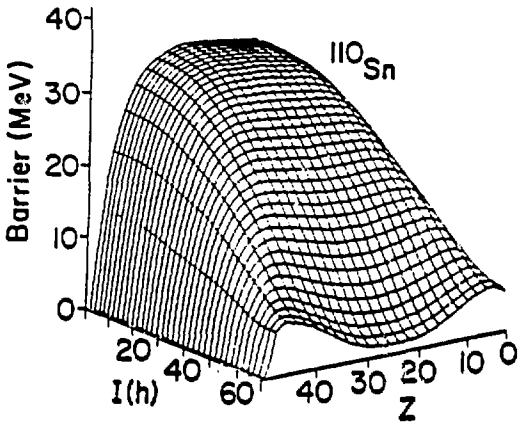

Figure 4. Surface plot of the asymmetry and angular-momentum-dependent barriers for the decay of $^{110}Sn^*$ calculated with a finite-range-corrected rotating liquid drop model[49].

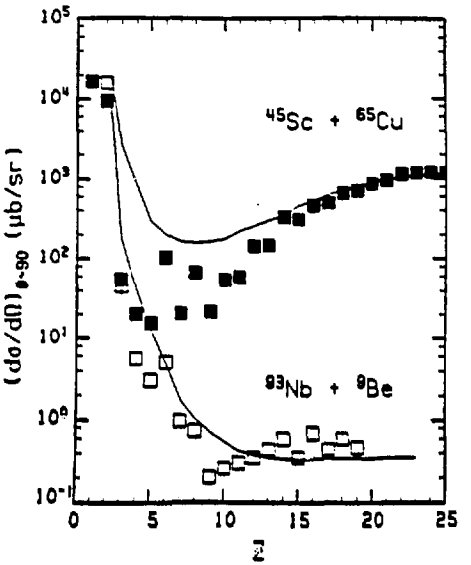

Figure 5. Differential cross sections for 200 MeV $^{45}Sc + ^{65}Cu$ (solid symbols) and 781 MeV $^{93}Nb + ^{9}Be$ (open symbols)[49]. The compound nuclei formed in the two reactions are very similar in mass and excitation energy, differing primarily in angular momentum.

the finite range model[49]. At zero angular momentum the nucleus is very close to the Businaro-Gallone point, and the ridge line is very flat. With increasing angular momentum, the Businaro-Gallone point moves downward and the ridge line develops a minimum at symmetry which becomes more pronounced as the angular momentum increases.

There is ample but scattered experimental evidence for the development of a minimum in the ridge line with increasing angular momentum[49], as seen in figure 5. Extensive evidence of the angular momentum dependence of the ridge line should come from the study of complex fragment emission throughout the periodic table.

4. ANGULAR MOMENTUM PARTITION BETWEEN FRAGMENTS: RIGID ROTATION AND ANGULAR MOMENTUM FRACTIONATION

The partition of the total angular momentum between the fragment spin and the orbital rotation is strongly affected by the mass asymmetry. In the limit of rigid rotation, the expected spin I_i of one of the fragments is:

$$I_i = \Im_i I_T / (\Sigma_i \Im_i + \mu d^2) \qquad (28)$$

where $\Im_i$ are the relevant fragment moments of inertia, μd^2 is the moment of inertia associated with the dinuclear system, and I_T is the total angular momentum.

This apparently trivial effect has been demonstrated in some reactions like Ne + Ag at 175 MeV[8]

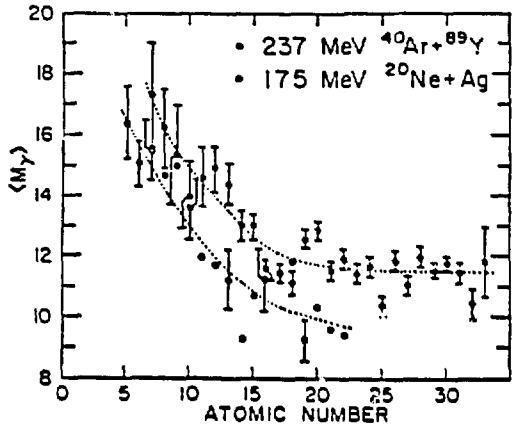

Figure 6. γ-ray multiplicity versus fragment atomic number for the reactions 175 MeV ^{20}Ne + ^{nat}Ag (open circles)[8] and 237 MeV ^{40}Ar + ^{89}Yb (filled circles) [9].

and Ar + Yb at 237 MeV[9], by measuring the γ-ray multiplicity (M_γ) as a function of mass asymmetry. M_γ should be approximately proportional to the sum of the fragment spins, and thus should increase with increasing asymmetry as predicted by (28). This signature is indeed seen in these reactions, as shown in figure 6. It is in fact seen more clearly in reactions like Kr + Ag[23] and Ar + Ni[21] where the spin of one of the two fragments was measured from the out-of-plane angular distributions of sequentially emitted alpha particles, as shown in figure 7. On the other hand, this signature is singularly absent in many other reactions where rigid rotation is expected because of the complete relaxation of the fragment kinetic energies[50-53]. In these reactions the total fragment spin is nearly independent of mass asymmetry (see figure 8).

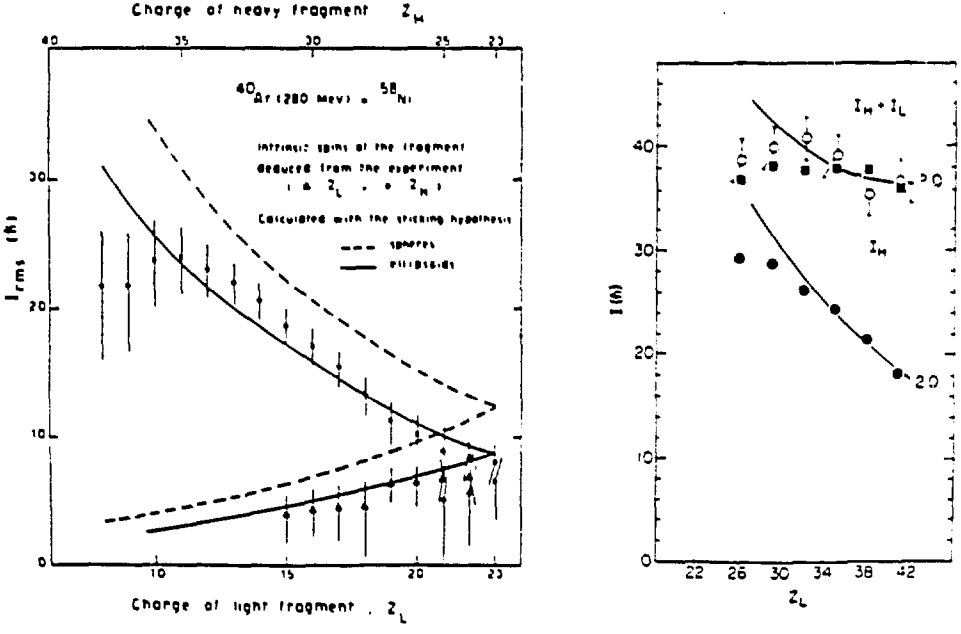

Figure 7. *(Left)* Experimental intrinsic spins of the individual fragments compared with the results of calculations for the sticking limit for rigid bodies[21]. *(Right)* The spin of the heavy fragment extracted from the α-particle angular distributions (full circles) and the sum of the spins inferred from the α-particle angular distributions (squares) and from M_γ data (open circles), for the reaction 664 MeV ^{84}Kr + ^{nat}Ag [23]. The lines correspond to rigid rotation calculations.

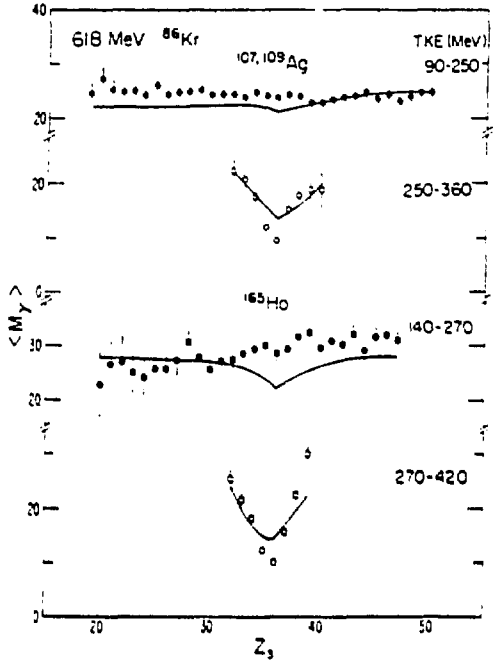

Figure 8. M_γ vs. atomic number for the reactions 618 MeV $^{86}Kr + ^{nat}Ag$ and 618 MeV $^{86}Kr + ^{165}Ho$. The full and the open symbols are data for a TKE gate on the deep inelastic and quasi- elastic reactions, respectively. The curves are diffusion model calculations[61].

The explanation for this apparent contradiction lies in what has been called angular momentum fractionation[32], namely a predominance of low ℓ-wave populations at large asymmetries. This fractionation of angular momentum along the mass-asymmetry coordinate can be one of two kinds. The first kind arises from statistical equilibration along the mass asymmetry coordinate[31]. The larger the ℓ-wave, the deeper the potential energy minimum at symmetry. As a consequence, high ℓ-waves should be concentrated in more nearly symmetric divisions, while low ℓ-waves should be spread out more evenly, and thus dominate at larger asymmetries[31].

The second kind is a dynamical fractionation typically associated with deeply inelastic processes[32]. The lower ℓ-waves are associated with a long interaction time and spread out their population to asymmetries far removed from that of the injection point, while the higher ℓ-waves are associated with a short interaction time and concentrate their strengths in the vicinity of the entrance channel asymmetry.

5. THE TILTING MODE AND FISSION FRAGMENT ANGULAR DISTRIBUTIONS

The standard assumption employed in calculating the fission fragment angular distribution is that the orientation in space of the saddle or scission configuration corresponds to the distribution of fragments at infinity. This is correct only in the limit in which the velocity arising from Coulomb repulsion is much greater than the velocity that the fragments possess because of their orbital rotation. Thus, this assumption is adequate for relatively small angular momenta, but should be used with caution in the case of the large angular momenta present in heavy ion reactions.

The role of the tilting mode in the angular distribution can be observed by substituting in the Gaussian K distribution: $K = I \cos\alpha$:

$$W(\alpha)\,d\Omega = W^0 \exp -\frac{I^2}{2T}\left[\frac{1}{\Im_\perp} - \frac{1}{\Im_c}\right] \exp\left[-\frac{I^2\cos^2\alpha}{2K_0^2}\right] d\Omega \,, \qquad (29)$$

where α is the emission angle, $K_0^2 = (\mathfrak{I}_{||}^{-1} - \mathfrak{I}_{\perp}^{-1})^{-1} T$, and $\mathfrak{I}_{||}, \mathfrak{I}_{\perp}$ are the principal moments of inertia of the saddle or scission configuration, and $\mathfrak{I}_c$ is the moment of inertia of the compound nucleus.

For a decay following complete fusion, the angular distribution becomes ($\Gamma_F < \Gamma_n$)[33]:

$$W(\theta) \propto \exp (- s_{max}) \left[I_0(s_m) + I_1(s_m) + \frac{\beta I_m^2}{2} \left\{ I_0(s_m) + \frac{2}{3} I_1(s_m) - \frac{1}{3} I_2(s_m) \right\} \right] \quad (30)$$

where $s_m = I_m^2 \sin^2\theta / 4K_0^2$, I_m is the maximum angular momentum, and I_0, I_1, I_2 are the modified Bessel functions of order 0, 1, 2. There are two interesting limits:

$$\lim_{p \to \infty} W(\theta) \propto (\sin \theta)^{-1} , \qquad \lim_{p \to 0} W(\theta) = \text{constant} \quad (31)$$

where $p = I_m^2 / 4K_0^2$.

An analysis of the fission-fragment angular distribution allows one to extract the quantity K_0^2 which, in turn provides information regarding the shape of the critical stage. What should this critical stage be? Early opinions favored the saddle point configuration, presumably because of its fundamental role in controlling the decay rate[5]. The reason why this configuration should be relevant to the angular distributions has never been made clear. Conservation of the K quantum number from saddle to scission is assumed, but there is no fundamental conservation law requiring it. The reasons advanced for the conservation of the K quantum number seem rather unconvincing. In fact, to at least one of the authors, such a K conservation appears little short of a miracle.

Miracle or not, early measurements at extremely low energies showed rapid variations of the angular distribution with changes of excitation energy in the 100 KeV range, which were interpreted in terms of discrete states at the saddle point with well-defined K quantum numbers[3,4]. At somewhat higher excitation energies, angular distributions and angular momenta seemed to be in accord with the statistical K distributions at the saddle, and the deduced moments of inertia appeared to agree with the saddle shapes predicted by the liquid drop model[2]. However, more recent data from fission induced by heavy ion reactions covering a broader range of excitation energies and angular momenta seem to be somewhat inconsistent with the predicted compact saddle shapes, and perhaps more in line with the more elongated scission configurations[37-46].

An alternative theory by Ericson[54], in which fission rates and angular distributions are predicted from the phase space of the fragments at infinity and the inverse cross section, has been revisited recently[42,43,45]. In a way, it could also be considered a "scission" theory. A comparison of the data with all three theories[55] seems to indicate that none is fully adequate to explain all the data and their energy dependence. An incomplete relaxation of the K quantum number from saddle to scission may be responsible for the observed features[56]. Unfortunately, knowledge of the relaxation times associated with this and possibly other degrees of freedom together with the knowledge of the transit time from saddle to scission are necessary to test this theory.

6. INTRINSIC ANGULAR - MOMENTUM - BEARING MODES: THEIR EFFECT ON THE MAGNITUDE AND ALIGNMENT OF THE FRAGMENTS SPIN

We have already illustrated how the thermal excitation of the bending, twisting, and wriggling modes can provide the fragments with spin, even when the total angular momentum is zero. This thermally-excited fragment angular momentum adds to that arising from rigid rotation, thus increasing the overall fragment spin, but, at the same time, introduces a misalignment of the fragment spin with respect to the normal of the fragment separation axis. The excitation of the tilting mode cannot provide any fragment spin if the total angular momentum is zero. However, it can increase the angular momentum of the fragments and can contribute to its misalignment. For instance, a full excitation of the tilting mode ($I = K$) leads to a complete transfer of the total angular momentum into fragment spin ($I_T = I_1 + I_2$) and to a spin alignment parallel, rather than perpendicular to the separation axis.

The first effect, an increase of the fragment spin over the amount expected from rigid rotation should be more evident in low angular momentum systems. It has been observed in a variety of reactions leading to fission, but also in many deeply inelastic reactions[57]. The observed fragment spin is always higher than that expected from rigid rotation, and seems to be consistent with the thermal excitation of the angular-momentum-bearing modes. Recent determination of the fragment spins based upon the measurement of discrete γ-ray lines associated with individual isotopes seems to indicate a high variability of the primary fragment spin, possibly associated with different shapes at the scission point[47].

The second effect, the fragment spin misalignment, is perhaps the most obvious expression of the excitation of the angular-momentum-bearing modes. It has been studied experimentally in rather extensive work on deeply inelastic reactions involving the measurement of in-plane and out-of-plane angular distributions of sequential fission fragments[25-29], or sequential γ-decay from the primary deeply inelastic fragments[11-20].

6.1. Angular Distribution of Sequentially Emitted Particles

The decay width of a particle as a function of the angle with respect to the angular momentum direction is given by (29). If the angular momentum has an arbitrary orientation with respect to our chosen frame of reference, defined by its components I_x, I_y, I_z, the angular distribution can be easily rewritten by noticing that:

$$K = I\cos\alpha = \hat{I} \cdot \hat{n} = I_x \sin\theta\cos\phi + I_y \sin\theta\sin\phi + I_z \cos\theta \ , \qquad (32)$$

where $\hat{n}$ is a unit vector pointing along the direction of particle emission with polar angles θ , ϕ . If the orientation of the angular momentum is controlled by the distribution in (23), we can integrate over the distribution of orientations and the fragment decay width becomes[58]:

$$\Gamma^J(\theta,\phi)\, d\Omega \propto \exp -\frac{I^2}{2T}\left[\frac{1}{\mathfrak{I}_\perp} - \frac{1}{\mathfrak{I}_c}\right] \frac{1}{S(\theta,\phi)} \exp -\left[\frac{I^2\cos^2\theta}{2\,S^2(\theta,\phi)}\right] d\Omega \qquad (33)$$

where:

$$S^2(\theta,\phi) = K_0^2 + (\sigma_x^2 \cos^2\phi + \sigma_y^2 \sin^2\phi)\sin^2\theta + \sigma_z^2 \cos^2\theta \ . \qquad (34)$$

In (33) we set $I_z = I$, in other words we average over the orientation but allow the decay width to depend upon only the average angular momentum, set equal to its z component. This expression should then be considered only as a high angular momentum limit ($\sigma // << 1$).

The final angular distribution is obtained by integrating over the fragment angular momentum distribution, which is assumed to reflect the entrance-channel angular momentum distribution. One obtains[58]:

$$W(\theta,\phi) = \frac{1}{S}\left[\frac{I_{min}^2}{A_{min}} \exp(-A_{min}) - \frac{I_{max}^2}{A_{max}} \exp(-A_{max})\right]. \qquad (35)$$

If $I_{min} = 0$, then:

$$W(\theta,\phi) = \frac{1}{SA}\left[1 - \exp(-A)\right] \qquad (36)$$

where:

$$A = A_{max} = I_{max}^2\left[\frac{\cos^2\theta}{2S^2} - \beta\right]; \ A_{min} = I_{min}^2\left[\frac{\cos^2\theta}{2S^2} - \beta\right]; \ \beta = \frac{1}{2T}\left[\frac{1}{\Im_n} - \frac{1}{\Im_\perp}\right]. \qquad (37)$$

The quantity $\Im_n$ is the moment of inertia of the nucleus after neutron emission, $\Im_\perp$ is the moment of inertia of the critical shape for the decay (e.g. saddle point). It is important to notice that the angular momentum dependence of the particle/neutron competition or fission/neutron competition is explicitly taken into account through β.

The final ingredient necessary for an explicit calculation of the angular distributions is the quantity K_0^2. This quantity can be expressed in terms of the principal moments of inertia of the critical configuration for the decay:

$$K_0^2 = \left[\frac{1}{\Im_{//}} - \frac{1}{\Im_\perp}\right]^{-1} T = \Im_{eff} T \ . \qquad (38)$$

For fission $\Im_{eff}$ can be taken from liquid drop calculations[1]. For light particle emission, the calculation of $\Im_{eff}$ can be worked out trivially.

6.2. Angular Distribution of Sequentially - Emitted γ- rays

Fragments with large amounts of angular momentum are expected to dispose of it mainly by stretched E2 decay. If the angular momentum of the fragment is aligned, the typical angular pattern of quadrupole radiation should be observed. Any misalignment should decrease the sharpness of this angular distribution. If the distribution of the angular momentum components I_x, I_y, I_z is

statistical, it is straightforward to derive an analytical expression for the angular distributions[52].

For a perfectly aligned system:

$$W(\alpha) = \frac{3}{4}(1+\cos^2\alpha)\ ; \qquad W(\alpha) = \frac{5}{4}(1-\cos^4\alpha)\ ; \tag{39}$$

For E1 For E2

If the angular momentum is not aligned with the z axis, one must express α in terms of θ and ϕ, which define the direction of the angular momentum vector. In particular:

$$\cos\alpha = \frac{\hat{I}\cdot\hat{n}}{I} = \frac{I_x \sin\theta\cos\phi + I_y \sin\theta\cos\phi + I_z\cos\theta}{(I_x^2+I_y^2+I_z^2)^{1/2}}\ . \tag{40}$$

For any given I, the angular distribution is obtained by integrations over the statistical distribution $P(\hat{I})$ of the angular momentum components:

$$W(\theta,\phi) = \int W(\alpha)\,P(\hat{I})\,d\hat{I}\ . \tag{41}$$

It is not possible to obtain an exact analytical expression for the general case. However, if we are willing to assume $\sigma_x^2 = \sigma_y^2 = \sigma_z^2 = \sigma^2$, then an exact result can be obtained. For the E1 distribution one obtains[58]:

$$W(\theta)_{E1} = \frac{3}{4}\left\{1+\cos^2\theta + \beta^2\left[1-D(\beta)\right](1-3\cos^2\theta)\right\}\ . \tag{42}$$

For the E2 distribution one obtains:

$$W(\theta)_{E2} = \frac{5}{4}\left\{1-\cos^4\theta - 2\beta^2\left[3\sin^2\theta\cos^2\theta - 2\cos^4\theta - \frac{3}{4}D(\beta)(\sin^2\theta - 4\cos^2\theta)\sin^2\theta\right]\right.$$
$$\left. - 3\beta^4(4\cos^4\theta + \frac{3}{2}\sin^4\theta - 12\sin^2\theta\cos^2\theta)[1-D(\beta)]\right\}\ . \tag{43}$$

In these equations $\beta = \sigma/\overline{I_z}$ and $D(\beta) = \sqrt{2}\beta\ F(\sqrt{1/2}\,\beta)$ where:

$$F(x) = e^{-x^2}\int_0^x e^{t^2}\,dt \tag{44}$$

is the Dawson's integral. One can verify immediately that both expressions behave as expected in the limits of $\beta = 0$ and $\beta = \infty$. The anisotropy $W(0^\circ)/W(90^\circ)$ tends to 1 when β tends to infinity for both E1 and E2 transitions, while it tends to 0 for E2 and to 2 for E1 when $\beta = 0$.

These results are graphically summarized in figure 9, where the anisotropy is plotted as a function of the fraction of E1 radiation for various values of $\sigma^2/\overline{I_z^2}$. The two extreme possibilities of stretched and nonstretched E1 decay are considered. If one has a fairly good experimental idea of the amount of E1 radiation to be expected from a given fragment and of its degree of stretching, the measurement of the anisotropy yields $\sigma^2/\overline{I_z^2}$, which is of course the most direct information about the misalignment.

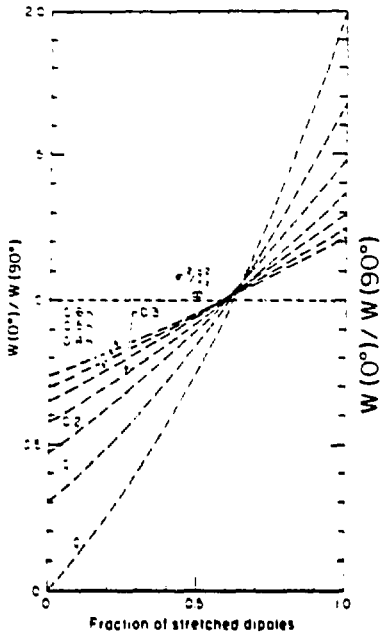

Figure 9. Calculated γ-ray anisotropies for mixtures of stretched E1 and E2 transitions as a function of the fraction of E1 radiation for various values of σ^2 / I_z^2 [58].

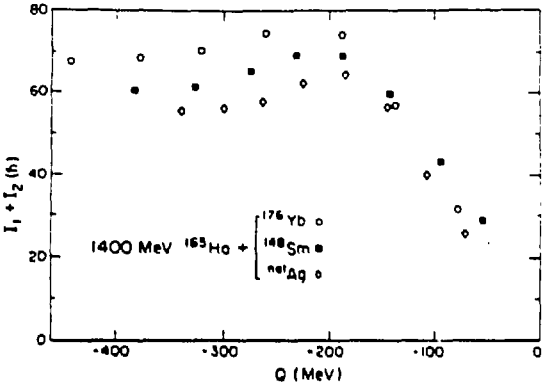

Figure 10. Sum of the spin magnitudes (I_1+ I_2) as a function of Q value for the reactions 1400 MeV ^{165}Ho + ^{nat}Ag,^{148}Sm and ^{176}Yb [20].

6.3. Experimental Spin Alignment from γ-Ray Angular Distributions

The continuum γ-ray anisotropy in heavy ion reactions has been extensively studied for the deep inelastic reaction 8.5 MeV/A Ho+Ho[18,19] and extended to the reactions 8.5 MeV/A Ho + Yb, Sm, Ag[20]. The Q-value spectrum was divided into a series of energy bins for which the γ-ray multiplicity, energy spectra, and anisotropy were measured.

The sum of the spins obtained from the γ-ray multiplicity as a function of Q value is shown in figure 10. As in other reactions[32], an increase in the energy loss leads to an initially rapid transfer of angular momentum to the fragments, followed by a relatively slow decrease as one moves toward the greatest inelasticities. These data (figure 10) show that each fragment can pick up as much as 35 - 40 ħ of angular momentum.

The anisotropy of the γ-rays (in the region of the γ-ray spectrum dominated by quadrupole radiation) as a function of Q value is shown in figure 11. In all cases, but more visibly for Ho + Yb, the anisotropy rises initially with increasing energy dissipation to values as high as two, and then declines slowly with further energy dissipation.

Qualitatively, the rise and fall of the γ-ray anisotropy with increasing energy dissipation is easily understood if studied simultaneously with the spin transfer. For small energy dissipations there is a small amount of angular momentum transferred to the fragments, which in turn can be easily depolarized by in-plane components arising from specific spectroscopic effects. As the energy dissipation increases, angular momentum is rapidly transferred to the fragments. This

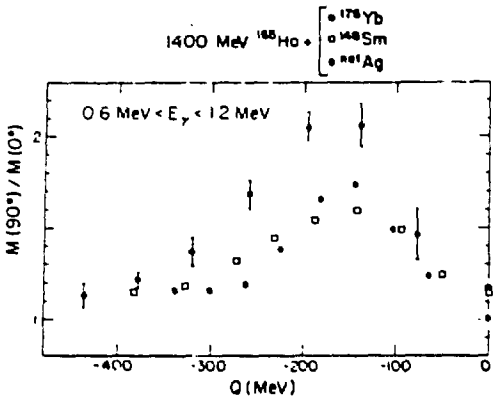

Figure 11. γ-ray anisotropy as a function of Q value for the reactions 1400 MeV ^{165}Ho + ^{nat}Ag, ^{148}Sm and ^{176}Yb, for heavy ions detected near the grazing angle. Error bars for the three systems are similar and are shown only for ^{165}Ho + ^{176}Yb [20].

transferred angular momentum is aligned and is little perturbed by the in-plane thermally-fluctuating components, which increase very slowly with excitation energy ($\sigma^2 \propto T \propto Q^{1/2}$). The resulting strong alignment is manifested in the substantial rise of the γ-ray anisotropy.

A further increase in the energy dissipation does not increase the transferred angular momentum but it increases the excitation energy and thus the thermal fluctuations of the in-plane components. As a consequence the total angular momentum becomes progressively less aligned and the γ-ray anisotropy decreases. Of course, there are additional sources of angular momentum misalignment, like particle evaporation from the primary fragments, but it appears that the main cause of angular momentum misalignment is the "thermal" excitation of the angular-momentum-bearing modes. The inclusion of thermal fluctuations provides us with picture almost coincident with the experimental data, as seen in figure 12. It should be pointed out that the calculation uses the experimental Mγ as input for the fragment angular momentum and uses

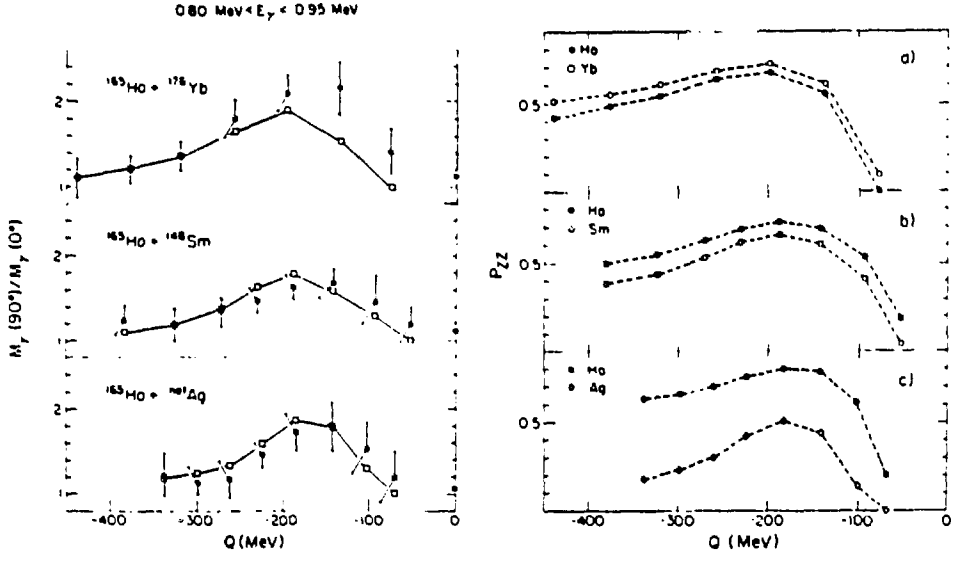

Figure 12. *(Left)* Comparison between experimental (circles) anisotropies of γ-rays (E = 0.8 - 0.95 MeV) in the reactions 1400 MeV ^{165}Ho + ^{nat}Ag, ^{148}Sm and ^{176}Yb [20] and a calculation based on the equilibrium statistical model (squares) as a function of Q value. Lines are drawn through the calculated points to guide the eye. *(Right)* Alignment parameter P_{zz} as a function of Q value, for each of the two inelastic fragments.

the theory only to calculate the σ's. In this way, the use of the theory may be valid even in Q-value regions where the full equilibrium limit has not been attained, since it is well known that fluctuations tend to their equilibrium limit a great deal faster than the average values[59].

From the above analysis one can calculate the alignment for each individual fragment, although this decomposition is far less certain that the calculation of the anisotropy. In figure 12 the alignment P_{zz} is shown for each of the two fragments. In general, alignments as great as 0.7 are observed, with the greatest alignments being associated with the heavier partner.

7. CONCLUSIONS

The relevance of the angular-momentum-bearing modes to the fission process at large is quite clear at this point, but specific understanding of their behavior is still somewhat elusive. More specifically, the outstanding question is: "Do the relevant observables reflect conditions frozen at the saddle point or at the scission point?" Fission decay widths seem to indicate that angular-momentum degrees of freedom depress the fission barriers and affect the transition state at the saddle point. However, fission angular distributions suggest K quantum numbers are frozen at the saddle point only for low energy and angular momentum, but not at higher energies and angular momenta. The intrinsic modes such as wriggling, bending and twisting should be relevant at scission. However, the most important experiments involving them have been carried out for deep inelastic reactions, and not for fission. Thus, the role of the angular-momentum-bearing modes in fission will remain an interesting and open question for quite a few years to come.

ACKNOWLEDGEMENTS

This work was supported by the Director, Office of Energy Research, Office of High Energy and Nuclear Physics, Division of Nuclear Physics of the U. S. Department of Energy under Contract DE-AC03076SF00098.

REFERENCES

1) S. Cohen, F. Plasil, and W. J. Swiatecki, Ann. Phys. 82 (1974) 557.

2) R. Vandenbosch and J. R. Huizenga, Nuclear Fission, (Academic Press, NY 1973) (and references therein).

3) A. Sicre, G. Barreau, R. Chastel, T. P. Doan, B. Leroux, and J. C. Sargeaux, Physics and Chemistry of Fission (Proc. Symp. Rochester NY), IAEA Vienna, (1974) 71.

4) A. Alm, T. Kivikas, and L. J. Lindgren, Physics and Chemistry of Fission (Proc. Symp. Rochester NY), IAEA Vienna, (1974) 55.

5) I. Halpern and V. M. Strutinski, Proceedings 2nd. U. N. Conference on the Peaceful Uses of Atomic Energy, United Nations, Geneva, 15 (1958) 408.

6) J. B. Wilhelmy, E. Cheifetz, R. C. Jared, S. G. Thompson, H. R. Bowman, and J. O. Rassmussen, Phys. Rev. C 5 (1972) 2041; A. Wolf and E. Cheifetz, Phys. Rev. C 13 (1976) 1952.

7) J. R. Nix and W. J. Swiatecki, Nucl. Phys. 71 (1965) 1; J. R. Nix, Nucl. Phys. A 130 (1969) 241; also J. R. Nix, PhD Thesis, Report UCRL-11338, (1964) unpublished.

8) P. Glässel, R. S. Simon, R. Diamond, R. C. Jared, I. Y. Lee, L. G. Moretto, J. O. Newton, R. Schmitt, and F. S. Stephens, Phys. Rev. Lett. 38 (1977) 331.

9) J. B. Natowitz, M. N. Namboodiri, P. Kasiraj, R. Eggers, L. Adler, P. Gonthier, C. Ceruti, and T. Alleman, Phys. Rev. Lett. 40 (1978) 751.

10) G. Wolschin and W. Nörenberg, Phys. Rev. Lett. 41 (1978) 691.

11) C. Lauterbach, W. Dünnweber, G. Graw, W. Hering, H. Puchta, and W. Trautmann, Phys. Rev. Lett. 41 (1978) 1774.

12) R. A. Dayras, R. G. Stokstad, C. B. Fulmer, D. C. Hensley, M. L. Halbert, R. L. Robinson, A. H. Snell, D. G. Sarantites, L. Westerberg, and J. H. Barker, Phys. Rev. Lett. 42 (1979) 697.

13) P. Aguer, R. P. Schmitt, G. J. Wozniak, D. Habs, R. M. Diamond, C. Ellegaard, D. L. Hillis, C. C. Hsu, G. J. Mathews, L.G. Moretto, G. U. Rattazzi, C. P. Roulet, and F. S. Stephens, Phys. Rev. Lett. 43 (1979) 1778.

14) M. N. Namboodiri, J. B. Natowitz, P. Kasiraj, R. Eggers, L. Adler, P. Gonthier, C. Ceruti, and S. Simon, Phys. Rev. C 20 (1979) 982.

15) H. Puchta, W. Dünnweber, W. Hering, C. Lauterbach, and W. Trautmann, Phys. Rev. Lett. 43 (1979) 623.

16) R. A. Dayras, R. G. Stokstad, D. C. Hensley, M. L. Halbert, D. G. Sarantites, L. Westerberg, and J. H. Barker, Phys. Rev. C 22 (1980) 1485.

17) R. J. Puigh, H. Doubre, A. Lazzarini, A. Seamster, R. Vandenbosch, M. S. Zisman and T. D. Thomas, Nucl. Phys. A 336 (1980) 279.

18) G. J. Wozniak, R. J. McDonald, A. J. Pacheco, C. C. Hsu, D. Morrissey, L. G. Sobotka, L. G. Moretto, S. Shih, C. Schuck, R. M. Diamond, H. Kluge, and F. S. Stephens, Phys. Rev. Lett. 45 (1980) 1081.

19) R. J. McDonald, A. J. Pacheco, G. J. Wozniak, H. H. Bolotin, and L. G. Moretto, C. Schuck, S. Shih, R. M. Diamond, and F. S. Stephens, Nucl. Phys. A 373 (1982) 54.

20) A. J. Pacheco, G. J. Wozniak, R. J. McDonald, R. M. Diamond, C. C. Hsu, L. G. Moretto, D. J. Morrissey, L. G. Sobotka, and F. S. Stephens, Nucl. Phys. A 397 (1983) 313.

21) R. Babinet, B. Cauvin, J. Girard, J. M. Alexander, T. H. Chiang, J. Galin, B. Gatty, D. Guerreau, and X. Tarrago, Z. Phys. A 295 (1980) 153.

22) W. Kuhn, R. Albrecht, H. Damjantschitsch, H. Ho, R. M. Ronningen, J. Slemmer, J. P. Würm, I. Rode, and F. Scheibling, Z. Phys. A 298 (1980) 95.

23) L. G. Sobotka, C. C. Hsu, G. J. Wozniak, D. J. Morrissey, and L. G. Moretto, Nucl. Phys. A 371 (1981) 510.

24) L. G. Sobotka, C. C. Hsu, G. J. Wozniak, G. U. Rattazzi, R. J. McDonald, A. J. Pacheco, and L. G. Moretto, Phys. Rev. Lett. 46 (1981) 887.

25) P. Dyer, R. J. Puigh, R. Vandenbosch, T. D. Thomas, and M. S. Zisman, Phys. Rev. Lett. 39 (1977) 392.

26) H. J. Specht, Proc. Int. Conf. on Nuclear Interactions, Australian Academy of Science, Canberra, Australia (1978).

27) P. Dyer, R. J. Puigh, R. Vandenbosch, T. D. Thomas, M. S. Zisman, and L. Nunnelley, Nucl. Phys. A 322 (1979) 205.

28) D. v. Harrach, P. Glässel, Y. Civelekoglu, R. Männer, and H. J. Specht, Phys. Rev. Lett. 42 (1979) 1728.

29) M. Rajagopolan, L. Kowalski, D. Logan, M. Kaplan, J. M. Alexander, M. S. Zisman, and J. M. Miller, Phys. Rev. C 19 (1979) 54.

30) G. J. Wozniak, R. P. Schmitt, P. Glassel, R. C. Jared, G. Blizard, and L. G. Moretto, Phys. Rev. Lett. 40 (1978) 1436.

31) L. G. Moretto and R. P. Schmitt, Phys. Rev. C 21 (1980) 204.

32) L. G. Moretto and G. J. Wozniak, Ann. Rev. Nucl. Sci. 34 (1984) 189.

33) L .G. Moretto, Nucl. Phys. A 247 (1975) 211.

34) L. G. Moretto and G. J. Wozniak, Prog. in Part. and Nucl. Phys. 38 (1988) 401.

35) U. L. Businaro and S. Gallone, Nuovo Cimento 1 (1955) 1277.

36) R. P. Schmitt and A. J. Pacheco, Nucl. Phys. A 379 (1982) 313.

37) B. B. Back, H. G. Clerc, R. R. Betts, B. G. Glagola, and B. D. Williams, Phys. Rev. Lett. 46 (1981) 1068.

38) B. B. Back, R. R. Betts, K. Cassidy, B. G. Glagola, J. E. Gindler, L. E. Glendenin, and B. D. Wilkins, Phys. Rev. Lett. 50 (1983) 818.

39) H. Rossner, D. Hilscher, E. Holub, G. Ingold, U. Jahnke, H. Orf, J. R. Huizenga, J. R. Birkelund, W. U. Schroder, and W. W. Wilke, Phys. Rev. C 27 (1983) 2666.

40) K. T. Lesko, S. Gil, A. Lazzarini, V. Metag, A. G. Seamster, and R. Vandenbosch, Phys. Rev. C 27 (1983) 2999.

41) P. D. Bond, Phys. Rev. Lett. 52 (1984) 414.

42) H. H. Rossner, J. R. Huizenga, and W. U. Schröder, Phys. Rev. Lett. 53 (1984) 38.

43) P. D. Bond, Phys. Rev. C 32 (1985) 471 and 483.

44) R. Freifelder, M. Prakash, and J. M. Alexander, Phys. Rep. 133 (1986) 315.

45) H. H. Rossner, J. R. Huizenga, and W. U. Schröder, Phys. Rev. C 33 (1986) 560.

46) J. M. Alexander, Ann. Phys. Fr. 12 (1987) 603.

47) T. L. Durrell, Workshop on Nuclear Structure, Copenhagen, May 16-20, 1988, unpublished.

48) A. J. Sierk, Phys. Rev. Lett. 55 (1985) 582.

49) L. G. Sobotka, D. G. Sarantites, Ze Li, E. L. Dines, M. L. Halbert, D. C. Hensley, R. P. Schmitt, Z. Majka, G. Nebbia, H. C. Griffen, and A. J. Sierk, Nucl. Phys. A 471, (1987) 131 (and references therein).

50) M. M. Aleonard, G. J. Wozniak, P. Glässel, M. A. Deleplanque, R. M. Diamond, L. G. Moretto, R. P. Schmitt, and F. S. Stephens, Phys. Rev. Lett. 40 (1978) 622.

51) A. Olmi, H. Sann, D. Pelte, Y. Eval, A. Gobbi, W. Kohl, U. Lynen, G. Rudolf, H. Stelzer, and R. Bock, Phys. Rev. Lett. 41 (1978) 688.

52) C. Gerschel, M. A. Delaplanque, M. Ishihara, C. Ngo, N. Perrin, J. Peter, B. Tamain, L. Valentin, D. Paya, Y. Susiyama, M. Berlanger, and F. Hanappe, Nucl. Phys. A 317 (1979) 473.

53) P. R. Christensen, F. Folkmann, O. Hansen, O. Nathan, N. Trautner, F. Videbaek, S. Y. Van Der Werf, H. C. Britt, R. P. Chestnut, H. Freiesleben, and F. Puhlhofer, Nucl. Phys. A 349 (1980) 217.

54) T. Ericson, Adv. Phys. 9 (1960) 425.

55) J. O. Newton, Preprint - Australian National University - P/1024 (1988).

56) V. S. Ramamurthy and S. S. Kapoor, Preprint - B. A. R. C., Trombay India, (1988).

57) R. P. Schmitt, G. Mouchaty, and D. R. Haenni, Nucl. Phys. A 427 (1984) 614.

58) L. G. Moretto, S. K. Blau, and A. J. Pacheco, Nucl. Phys. A 364 (1981) 125.

59) L. G. Moretto, LBL Report No. LBL-12596, Berkeley (1981).

60) D. J. Morrissey, G. J. Wozniak, L. G. Sobotka, A. J. Pacheco, R. J. McDonald, C. C. Hsu, and L. G. Moretto, Nucl. Phys. A 389 (1982) 120.

61) R. Regimbart, A. Behkami, G. J. Wozniak, R. P. Schmitt, J. S. Sventek, and L. G. Moretto, Phys. Rev. Lett. 41 (1978) 1355.